Simulation of the cross-correlated in-plane tow centroid of textile composites based on experimental data.

Andy Vanaerschot[a,*], Brian N. Cox[b], Stepan V. Lomov[c], Dirk Vandepitte[a]

[a] *KU Leuven, Dept. of Mechanical Engineering, Leuven, Belgium*
[b] *Teledyne Scientific Co. LLC, Thousand Oaks, CA, USA*
[c] *KU Leuven, Dept. of Metallurgy and Materials Engineering, Leuven, Belgium*

Abstract

In-plane centroids of textile composites are simulated as cross-correlated random fields. Each tow position is defined as an average trend quantified from experimental data, added with zero-mean deviations produced as a stochastic field. Realisations of these fields are generated using a framework based on the Karhunen-Loève series expansion that is calibrated with experimental information from prior work. Positional deviations are obtained that are correlated along the tow and between neighbouring tows.

The application is a 2/2 twill woven carbon fibre reinforced epoxy consisting of multiple unit cells. Generated in-plane deviations of the warp and weft tows resemble the experimental fluctuations with similar wavelengths. Simulation of thousand specimens demonstrates that the virtual in-plane positions possess the experimental standard deviation and correlation lengths on average.

Keywords: Textile composites, Multi-scale modelling, Non-determinism, Probabilistic methods

*Corresponding author. Department of Mechanical Engineering, Katholieke Universiteit Leuven, Celestijnenlaan 300B, 3001 Heverlee, Belgium. Tel.:+32 16372779 ; fax:+32 16322838

Email address: Andy.Vanaerschot@mech.kuleuven.be (Andy Vanaerschot)

1. Introduction

The reinforcement structure of a textile composite is susceptible to a significant amount of variability. Though, component-scale composites are often modelled using identical tow path descriptions and repetitive application of identical unit cells. Such ideal representations do not appear in physical samples and lead to unreliable results when performing simulations. A correct identification of the spatial geometrical fluctuations of a textile product improves the quality of numerical analyses and permits to quantify the effect of variability on the mechanical performance.

This deficiency in realistic simulations is partially attributed to the lack of experimental data with a thorough statistical analysis. Researchers who are quantifying the variation in geometry usually do not consider correlation. However, the description of dependency between a single property at a certain location or between different parameters at one location, is required to reproduce the correct geometry of the material. This is already demonstrated for several types of composites [1]. Further, modelling techniques are often inadequate to introduce local and long-range variations in the tow path and accurately simulate the desired correlation structures [2]. It is not the objective to simulate more precise representations without considering experimental data, such as in [3], but to calibrate the numerical modelling procedure with the measured variations. Realistic representations of textile composites are acquired by a two-step procedure [4]: (i) collection of sufficient experimental data on the spatially correlated short- and long-range geometrical variations, and (ii) derivation of the macroscopic mechanical properties from the lower scale geometrical characteristics. This paper describes the last step of the approach of Charmpis et al. [4] and is preceded by several other publications [5, 6, 7]. A methodology is proposed to generate the long-range geometrical variability of textiles, and is demonstrated for a 2/2 twill woven carbon fibre reinforced epoxy composite.

Long-range variations are mostly omitted when modelling component-size textile samples. Generally, representative volume elements are assembled to generated any size of composite, but this is not a full replica of the real reinforcement structure. Simulation of long-range variations in textile composites is only sparsely tackled in literature. Skordos and Sutcliffe [8] investigated the in-plane behaviour of a carbon-epoxy satin weave for modelling the forming process. Tow orientations are simulated as an Ornstein-Uhlenbeck process of which the parameters are estimated by the likelihood function. Next, realisations of woven sheets are obtained using the Cholesky decomposition of the covariance structure of warp and weft direction in combination with normally distributed independent variables. Values of warp and weft orientation and unit cell size are generated at discrete points that compromise the warp and weft direction and size of the unit cell. Endruweit et al. [9] performed stochastic injection simulations in bi-directional non-crimp fabrics. Random fields of fibre distances are constructed using spectral representations with trigonometric functions to implement spatial correlation along the tow. The frequency and phase of each function are determined randomly on given intervals, with an upper limit for frequencies determined by the fabric mobility in the transverse direction observed in actual fabrics and the phases between 0 and π. Abdiwi et al. [10] reproduced full-field variability of the tow directions across flat sheets based on measured variability of inter-tow angles. The geometry mesh is generated with a pin-jointed net kinematics code where variability is added by stretching and additional perturbations of the nodes. These perturbations are introduced using sinusoidal functions with particular wavelength and vertical amplitude to simulate the long-range correlation effects. No short-range variability is considered. This code is implemented in a genetic algorithm with objective functions that minimises the mean and standard deviation of the measured inter-tow angle to reproduce similar statistical variations as measured. Series expansion techniques are also employed by Yushanov and Bogdanovich [11] to generate a random reinforcement path

characterised by its mean value and covariance matrix. The stochastic reinforcement is generated by defining a suitable position vector with a random vector function which is expanded into a deterministic component and a random component. A stochastic local basis is afterwards introduced to uniquely define the directional cosines of the arbitrary reinforcement path, specified by the position vector.

Except for the contribution of Skordos and Sutcliffe, all described publications consider an approximated correlation function along the tow direction which is not validated with experimental data. The presence of cross-correlation between neighbouring tows is also not tackled or is indirectly introduced. Experimental validation of the input data and correct introduction of all correlation structures are however mandatory to replicate the internal geometry. To precisely model the long-range tow path parameters, a methodology developed by Vořechovský [12] is chosen which is not yet applied in the field of composites. Vořechovský proposed a framework for generating cross-correlated random fields based on Karhunen-Loève series expansion. Each random field must share an identical auto-correlation, while the cross-correlation structure between each pair of fields can be described by a simple coefficient.

This paper discusses the implementation of the procedure of Vořechovský for generating Gaussian random fields of the in-plane centroid. The methodology is calibrated with the experimental data of [7]. In summary, the objectives of the paper are to (i) apply the method of Vořechovský [12] in the field of textile composites, (ii) simulate the in-plane positions of warp and weft tows, and (iii) compare the experimental and simulated statistical information.

2. Experimental data

The developed methodology is demonstrated for a 2/2 twill woven Hexcel fabric (G0986) [13] impregnated with epoxy resin. Each reinforcement is built with four equally spaced warp and weft tows consisting of 6K carbon fibres, with a nominal areal

density of 285 g/m^2. The idealised unit cell topology is given in figure 1 with λ_x=11.43 mm and λ_y=11.43 mm, respectively the periodic lengths of warp (x-axis) and weft (y-axis) tows as specified by the manufacturer.

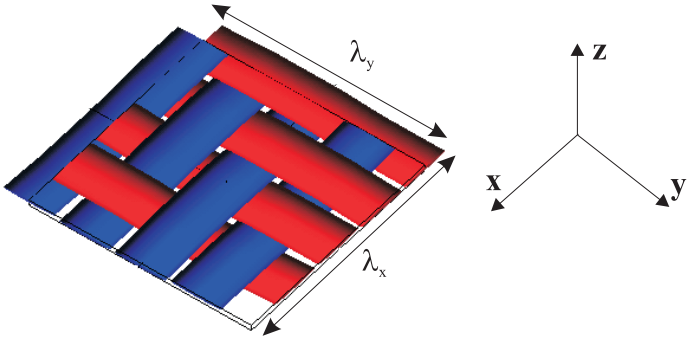

Figure 1: WiseTex model of a 2/2 twill woven reinforcement. The x-axis and y-axis of the coordinate system are respectively parallel to the warp and weft direction.

Data of the in-plane centroid is collected in [7] from two single-ply carbon fabrics impregnated with epoxy in a resin transfer moulding (RTM) process. The in-plane dimension of both samples (sample 1 & 2) is quantified using optical imaging over a square region of thirteen by thirteen unit cells to investigate the long-range effect. In-plane positions of forty warp and forty weft tows are derived that represent a total of hundred unit cells by manually marking the boundaries of tows for prescribed grid spacings. Centroid locations are subsequently defined as half the tow width at each grid location. These coordinates are given as input to Matlab where they are transformed to a global axis system and compensated for possible misalignment during scanning.

The digital image of sample 1 in figure 2 shows that the in-plane centroid of a single tow does not follow a straight path over the entire sample. The dots in the image, representing the in-plane tow path, clearly deflect from the straight dashed line. The in-plane movement in transverse direction of the path is quantified by computing the difference between the experimental tow paths and a best-fitted ideal lattice description. Tows of this lattice are represented as straight lines, with nominal spacing in x- and

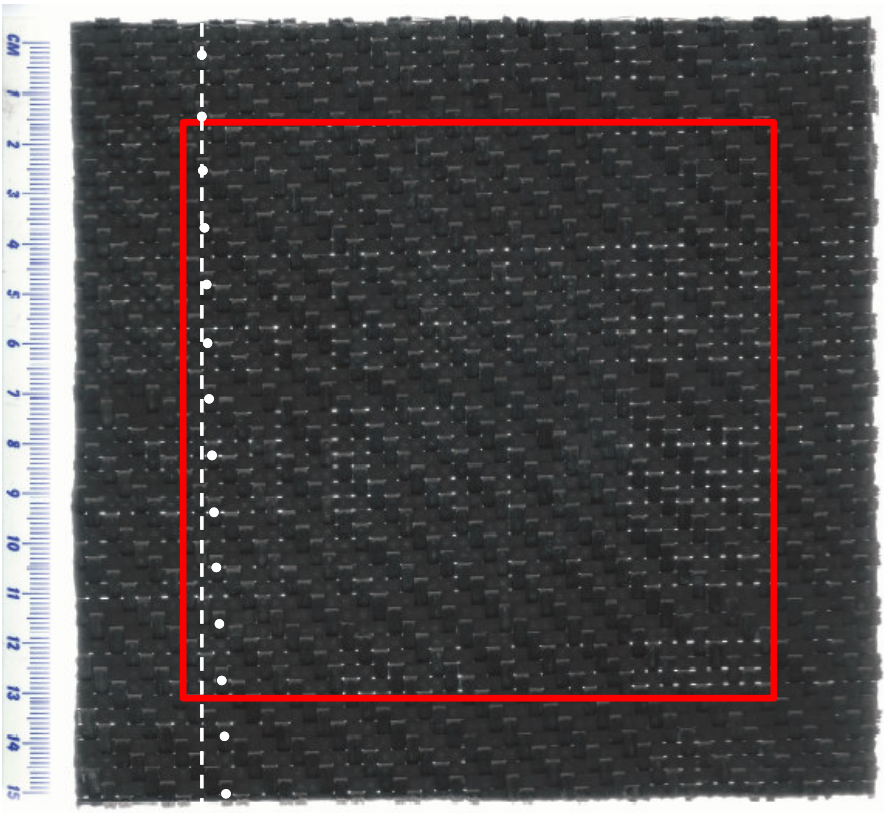

Figure 2: Optical scan of a one-ply 2/2 twill woven carbon fibre fabric impregnated with epoxy resin. Warp tows are oriented horizontally, while weft tows are positioned in vertical direction. The red square indicates the region where the in-plane position is characterised.

y-direction derived from the experimentally obtained periodic lengths. The in-plane warp and weft fluctuations are considered respectively in y- and x-direction.

The obtained deviations are represented as $\varepsilon_i^{(j,t,s)}$, with i the grid location ($i = 1..N_i$, $N_i = 40$), j the tow index ($j = 1..N_f$, $N_f = 40$) in each direction, t= warp or weft tows and s=1 or 2 referring to the sample. A non-periodic trend along the tow length is observed which presumably originates from the handling of the material during storage, cutting and placement in the RTM mould. This trend $< \varepsilon_i^{(j,t,s)} >$ (see figure 6) is determined as the average value per grid location of all in-plane deviations in one

sample. Next, in-plane deviations $\varepsilon_i^{(j,t,s)}$ are decomposed in:

$$\varepsilon_i^{(j,t,s)} = < \varepsilon_i^{(j,t,s)} > + \zeta_i^{(j,t,s)} \tag{1}$$

with $\zeta_i^{(j,t,s)}$ the stochastic variations attributed to the loom itself, further referred as *deviations*. The stochastic variations of sample 1 and 2 are combined in one larger data set per tow type $\zeta_i^{(j,t)}$, assuming that no physical differences are present between the $\zeta_i^{(j,t,s)}$ of the samples. Considering the weaving process of the 2/2 twill woven fabric, the warp tows can be represented by one representative tow, called *genus*, and similar for the weft tows. The experimental deviations $\zeta_i^{(j,t)}$ are presented in figure 3 showing that the in-plane warp deviations have a short wavelength, while the weft in-plane centroids fluctuate with a longer wavelength.

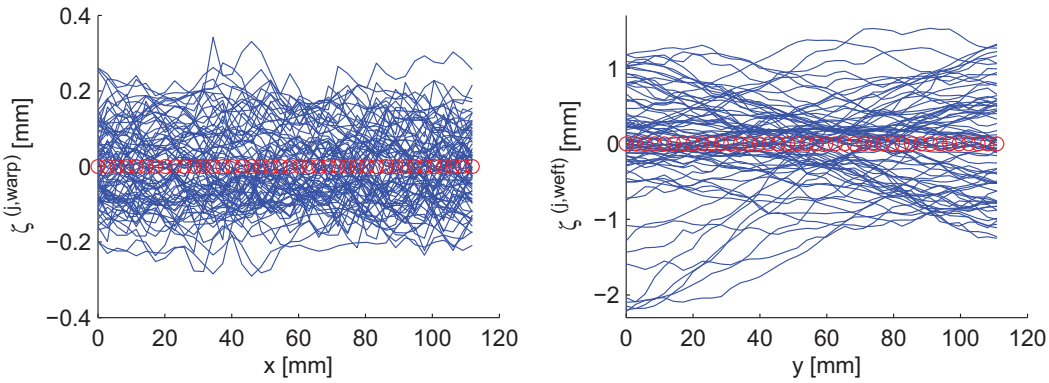

Figure 3: Experimental deviation trends $\zeta^{(j,t)}$ of warp (left) and weft (right) tows.

In contrast to the short-range variations in [5], which are fairly represented by normal distributions, in-plane deviations $\zeta_i^{(j,t)}$ show large deflections from normality. Especially the weft deviations seem to follow a particular distribution. However, from the limited amount of samples it is not possible to verify if another type of distribution could be more relevant. Any small shift in periodicity during fabric production already results in a very different weft tow spacing for such samples. The assumption of normality is

still acceptable as is indicated by the kurtosis and skewness values [1] in table 1. Warp in-plane deviations are well approximated by a normal distribution, with the largest differences occurring in the tails where a lower frequency is present.

Table 1: Skewness and kurtosis values of stochastic in-plane deviations.

	normal distribution	warp tows	weft tows
Kurtosis	3	2.49	3.83
Skewness	0	0.18	-0.52

The statistical behaviour of the deviations $\zeta_i^{(j,t)}$ are further described in terms of standard deviation σ and correlation information. Correlation is investigated using the Pearson's moment correlation parameter for pairs of data (or *lags*) taken at distinct locations on a single tow (*auto-correlation* C_A), and pairs of data on neighbouring tows but fixed at the same grid location on a tow (*cross-correlation* C_C). Definitions of both correlation directions are given in figure 4. The appearing trend in the correlation graphs are fitted using exponential and squared exponential correlation functions to estimate the correlation length ξ, which is a measure of the range over which fluctuations at a certain position still have an influence on the fluctuations at another location. This fitting procedure only considers the first twenty lags which corresponds to the length of five unit cells. Larger point spacings are not used to fit a correlation trend since these data are based on a smaller data set size and thus subjected to a larger variability. The auto- and cross-correlation behaviour is well represented by an exponential correlation function for the warp in-plane deviations, while the squared exponential function is a better fit for both correlation directions of the weft tows.

Variation in the in-plane centroid, indicated by the standard deviation, is five times

[1] The skewness describes the lack of symmetry in the distribution, while the kurtosis value refers to the peakedness of the distribution

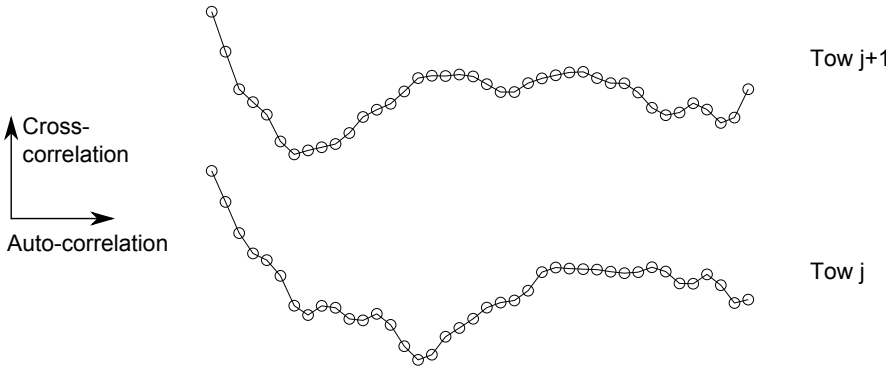

Figure 4: Definition of spatial dependencies of deviations demonstrated for two weft tows: auto-correlation (along the tow) and cross-correlation (between neighbouring tows).

higher for the weft direction. The in-plane warp correlation length ξ_A along the tow is approximately twice of the weft tows, reflecting the tensioning of the warp tows and the lack of tensioning of the weft tows during production. Individual weft tows are less controlled in their path, leading to bundling of neighbouring weft tows as observed in figure 2. This effect is translated in a higher cross-correlation length ξ_C for the weft tows, exceeding the unit cell dimension. A more detailed discussion of the procedure and results is given in [7].

Table 2: Standard deviation, auto- and cross-correlation lengths of the in-plane centroid using the combined data set.

	Warp tows	Weft tows
σ [mm]	0.106	0.615
ξ_A [mm]	114.89	52.89
ξ_C [mm]	4.49	13.16

3. Simulation of the in-plane centroids

3.1. Overview

The in-plane centroids of a thousand virtual textile models are generated that consist of forty warp and weft tows. Each tow length is discretized in forty-one equidistant points such that the length between five consecutive grid locations corresponds to the periodic length of the warp or weft tow (figure 5). This limited amount of grid locations is sufficient to represent the in-plane centroid since no short-range variations are observed in the unit cell sample of [5]. A stochastic description of the tow path is obtained by combining the experimental handling trend with cross-correlated long-range deviations. These deviations are simulated as random fields using the statistical information of section 2. Warp and weft in-plane deviations are generated independently, assuming that the deviations are normally distributed.

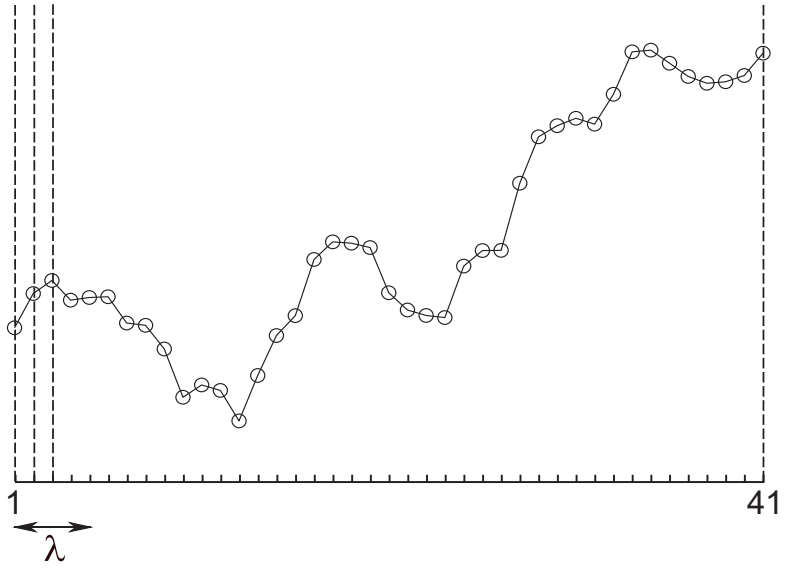

Figure 5: Grid representation of the simulated in-plane deviations.

3.2. Handling trend

Figure 6 presents the average trend $< \varepsilon_i^{(j,t,s)} >$ of the in-plane warp and weft genus. As discussed in section 2, the lack of periodicity signifies that this tendency should not be interpreted as a systematic trend, representing the repetitive mean behaviour of the tow path, but as an effect due to handling. Zero-mean deviations are added to the handling trend to obtain random realisations of the in-plane positions.

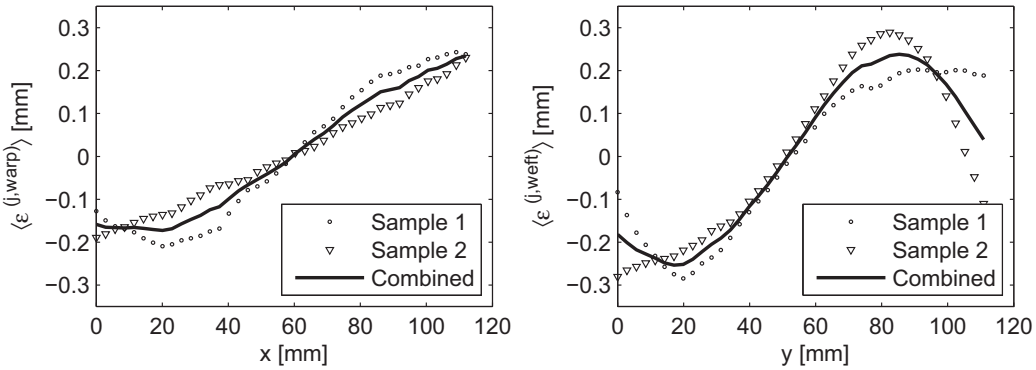

Figure 6: Handling trend of warp (left) and weft (right) tows.

3.3. Long-range in-plane deviations

Reproducing the long-range statistics requires a simultaneous generation of all in-plane deviations belonging to the same genus within a single specimen. This strategy is assimilated in a methodology by Vořechovský [12] where cross-correlated material properties of a concrete structure are simulated. The procedure is however generally applicable for the modelling of a set of stochastic fields which share an identical auto-correlation structure and of which the cross-correlation can be defined by a cross-correlation coefficient. The method is a generalisation of the simulation of independent distinct one-dimensional (1-D) or *univariate* random fields to cross-correlated univariate fields, further referred as *multivariate* fields. First a brief description of univariate fields is given to understand the principles used in the procedure of Vořechovský.

3.3.1. Description of the methodology

A stochastic property is described by a univariate random field $H(x, \theta)$ [14] that represents its spatially correlated behaviour, with θ demonstrating the randomness. Different realisations of this field can be simulated using series expansion techniques [15, 16]. These discretise the stochastic field $H(x, \theta)$ by expanding any realisation using a set of random variables $\mu_i(\theta)$ and deterministic spatial functions $g_i(x)$ that represent the auto-correlation structure:

$$H(x, \theta) = \sum_{i=1}^{\infty} \mu_i(\theta) g_i(x) \tag{2}$$

In the case of the Karhunen-Loève (K-L) series expansion, these deterministic functions $g_i(x)$ are obtained by spectral decomposition of the auto-correlation function $C_A(x, x')$:

$$C_A(x, x') = \sum_{i=1}^{\infty} \lambda_i^A \phi_i^A(x) \phi_i^A(x') \tag{3}$$

with λ^A and ϕ^A respectively the eigenvalues and eigenvectors of the auto-correlation structure, acquired by solving the eigenvalue problem. Any realisation of the zero-mean random field $H(x, \theta)$ can now be presented as:

$$H(x, \theta) = \sum_{i=1}^{\infty} \sqrt{\lambda_i^A} \eta_i(\theta) \phi_i^A(x) \tag{4}$$

with $\{\eta_i, i = 1..\infty\}$ a set of independent orthonormal random variables. In practice, a truncation of the random field $H(x, \theta)$ is performed by using a finite set of random variables $\{\eta_i, i = 1..N_A\}$. The number of K-L terms N_A in the series is defined by ordering the eigenvalues in a descending series and considering only the N_A larger eigenvalues that capture most of the randomness. The eigenvector basis $\phi_i^A(x)$ in the K-L expansion is optimal in the sense that the mean-square error resulting from a finite

representation of $H(x,\theta)$ is minimised. For sufficiently large N_A, the second-moment properties of $H(x,\theta)$ can thus be approximated by the second-moment properties of $\hat{H}(x,\theta)$:

$$\hat{H}(x,\theta) = \sum_{i=1}^{N_A} \sqrt{\lambda_i^A}\eta_i(\theta)\phi_i^A(x) \tag{5}$$

For more information about the K-L series expansion and its properties, the reader is referred to [15, 16]. This simulation technique is already applied to generate individual auto-correlated composite properties: stiffness properties of twintex composites [1], volume fraction of long fibre thermoplastic material [17] and material properties of laminated composites in [18].

The framework of Vořechovský enables to simulate cross-correlated random fields using the K-L series as basis. The key idea of the method is that all cross-correlated fields, within a single specimen, are expanded using the same spectrum of eigenvectors, but the sets of random variables used for the expansion of each field are cross-correlated with neighbouring fields. These latter sets must be correlated with respect to the cross-correlation function. The subsequent steps to produce N_{sim} realisations of Gaussian cross-correlated fields are:

1. Perform modal decomposition of the auto-correlation structure and apply truncation: λ_i^A, $\phi_i^A(x)$ with $i = 1..N_{var}$ $(N_{var} \leq N_A)$
2. Perform modal decomposition of the cross-correlation structure and apply truncation: λ_i^F, $\phi_i^F(x)$ with $i = 1..N_{f,r}$ $(N_{f,r} \leq N_F)$
3. Generate $N_r \times N_{sim}$ $(N_r = N_{var} \cdot N_{f,r})$ Gaussian uncorrelated random variables η_r using Latin Hypercube Sampling (LHS)
4. Construct the cross-correlated random matrix $\chi^D = \phi^C \lambda^C \eta_r$ of which the elements are uncorrelated for a single tow and cross-correlated between tows

5. Simulate all individual random fields for a single realisation by

$$\hat{H}_j(x,\theta) = \sum_{i=1}^{N_A} \sqrt{\lambda_i^A}\chi_{j,i}^D \phi_i^A(x) \tag{6}$$

Modal decomposition of the correlation functions is performed in the same way as equation 3, with N_A equal to the number of grid locations to represent a single random field and N_F the number of fields which are cross-correlated. The independent random variables η_r are generated using LHS which is a special type of Monte Carlo simulation. In LHS, stratification of the theoretical probability distribution function is performed to limit the number of simulations. The s-th realisation ($s = 1..N_{sim}$) of the random variable η of location i ($i = 1..N_{var}$) is computed using:

$$\eta_{i,s} = F_i^{-1}\left(\frac{\pi_j(s) - rand}{N_{sim}}\right) \tag{7}$$

with F^{-1} the inverse of the cumulative normal distribution function, π a random permutation of $1..N_{sim}$, and $rand$ a random uniform distributed number. The cross-correlated matrix χ^D is built using the eigenvalue decomposition method and such that it consists of j blocks ($j = 1..N_f$), where each block consists of N_{var} standard Gaussian independent random variables, while the vectors χ_i^D and χ_j^D are cross-correlated. This is the most important step in the procedure and reproduces the cross-correlation structure between the different N_f random fields. The random field expression of each property or parameter is expanded using the same formula of equation 5 but now with $\chi_{j,i}^D$ as random variables. All the produced fields will possess the correct auto- and cross-correlation structure between neighbouring fields. A detailed description of the procedure is elaborated in [12].

Vořechovský also proposes additional operations that could enhance the accuracy: (i) application of correlation control techniques and (ii) generation of additional side

points. The first procedure encounters the problem of spurious correlation which is sometimes introduced along the random variables $\chi_{j,i}^{D}$ of a single field representing tow j. This could alter the resulting correlation information of the generated deviations. To assess the effect, techniques to diminish the undesired correlation are proposed in [19]. However, no apparent difference is observed using correlation control for the simulation of the 2/2 twill in-plane position. Omitting such operation significantly downsizes the computational expense and will thus not be considered. Additional side points are considered in case disturbances are present in the generated values at the edges. However, no effect is observed in the produced in-plane deviations of section 3.3.2, so no additional grid locations are anticipated.

3.3.2. Application to the in-plane centroid deviations

The in-plane centroid deviations are generated using the framework of Vořechovský. A single tow is represented over a grid of forty-one points ($N_A = 41$) by a zero-mean Gaussian random field that shares the same correlation structure along the tow and of which the random variables are cross-correlated with neighbouring tows of the same genus. Warp and weft simulations are performed separately, with each realisation consisting of forty individual but cross-correlated fields ($N_f = 40$). The target statistics are reproduced by projecting the correlation functions, given in table 3, onto the equidistant grid of figure 5. From this information, auto- and cross-correlation matrices are constructed. Since the mean and variance are constant over the field and correlation is only dependent on the distance between two points ($\tau = x_2 - x_1$), the generated stochastic fields are *homogeneous*.

Random fields H_j of the in-plane centroids are computed using the truncated series in equation 6. After sorting the eigenvalues in descending order, only the N_{var} or $N_{f,r}$ largest eigenvalues and corresponding eigenvectors are considered. An appropriate measure of the captured variability, as discussed in section 3.3.1, is given by normalised

Table 3: Input correlation functions for simulating the in-plane fluctuations.

	Warp tows	Weft tows
Auto-correlation C_A	$\sigma_{wa}^2 \exp(-\frac{\tau}{\xi_{wa,A}})$	$\sigma_{we}^2 \exp(-\frac{\tau^2}{\xi_{we,A}^2})$
Cross-correlation C_C	$\exp(-\frac{\tau}{\xi_{wa,C}})$	$\exp(-\frac{\tau^2}{\xi_{we,C}^2})$

sum (or truncation error) δ which is fixed to minimum 0.9975:

$$\delta = \frac{\sum_{i=1}^{N_{red}} \lambda_i}{\sum_{i=1}^{N} \lambda_i} \geq 0.9975 \tag{8}$$

with N_{red} equal to N_{var} or $N_{f,r}$. The normalised sum δ over all eigenvalues is shown in figure 7 for the warp and weft tows with the resulting truncation parameters given in table 4. Considering truncation is computationally advantageous for the weft in-plane positions, while it is limited or even not possible for the warp in-plane centroid, given the maximum chosen truncation error δ.

Table 4: Truncation parameters of the series expansion method.

	N_{var}	$N_{F,r}$
Warp tows	33	40
Weft tows	4	13

In-plane deviations are produced for 40000 warp and weft tows as mentioned in section 3.1. The produced zero-mean deviations trend of an arbitrary specimen in figure 8 demonstrates a good agreement with the experimental in-plane deviations shown in figure 3; the short wavelength of the experimental warp fluctuations and long wavelength of the measured weft deviations are reproduced in the simulated data. The deviations possess fewer low-amplitude short-range fluctuations than observed in the experiments. This is not only attributed to the series expansion method, but also to the normal-

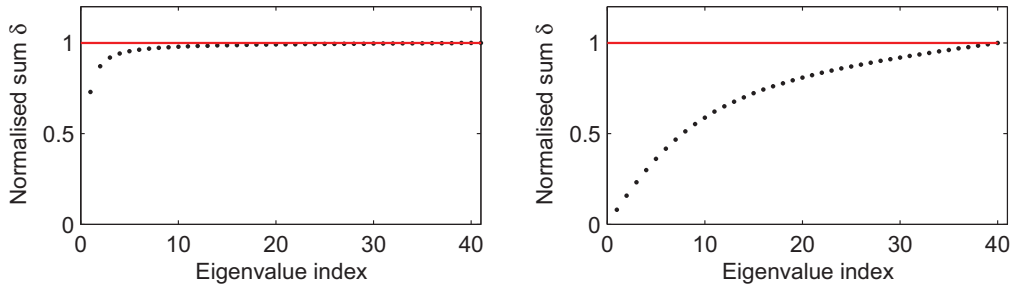

(a) Warp tows

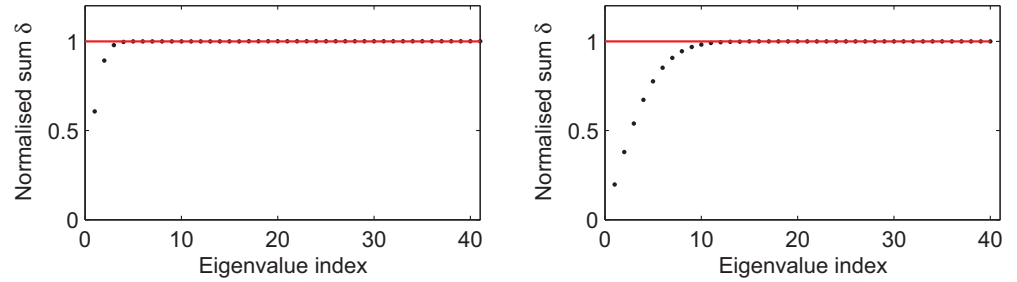

(b) Weft tows

Figure 7: Normalised sum δ of the eigenvalues of the auto-correlation (left) and cross-correlation (right). The red line indicates when the normalised sum is equal to 1.

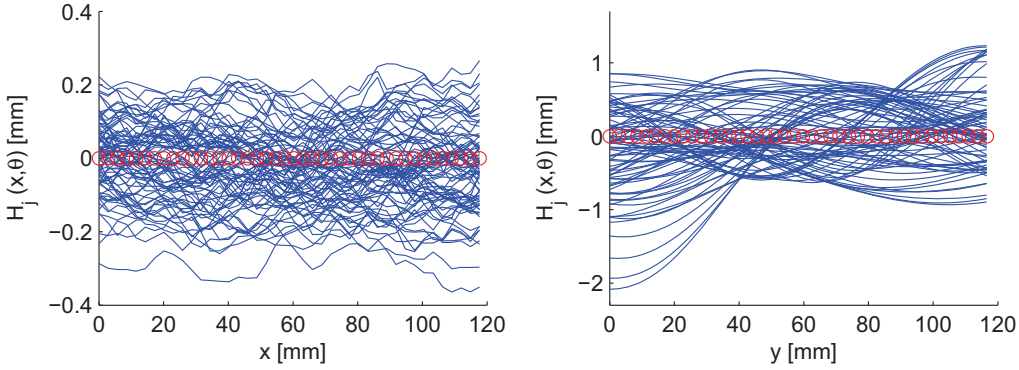

Figure 8: Simulated warp (left) and weft (right) deviations trend for 80 warp and weft tows.

ity assumption of the in-plane deviations which diminish the presence of large short wavelength oscillations in the simulations.

The deviations also have comparable patterns in neighbouring mean tow orientations, defined by the slope of a linear least-square fit to all deviation values along a single tow. Specifically for the weft in-plane positions, neighbouring weft tows possess similar orientations due to the significant cross-correlation as presented in figure 9. The simulated trend is more regular which is again caused by the assumption of a normal distribution for the in-plane centroid deviations. No such patterns are observed for the warp in-plane deviations which have a lower standard deviation and limited cross-correlation.

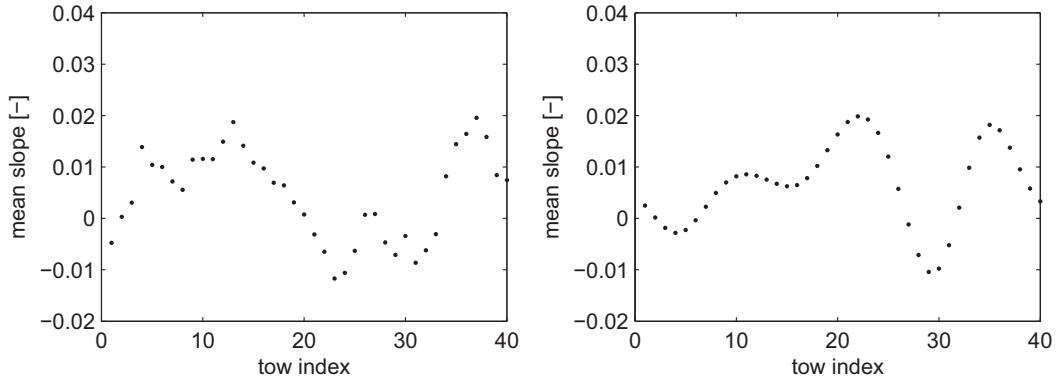

Figure 9: Mean tow orientations of weft in-plane deviations: experimental trend of sample 2 (left) vs. simulated trend of an arbitrary specimen (right).

The corresponding statistics to the thousand generated virtual specimens are verified in each tow direction for (i) the combined data set, (ii) individual specimens consisting of hundred unit cells and (iii) individual 1-D random fields representing a single tow with a length of ten unit cells. The normalised difference Δ from the target values in table 2 is defined as $\Delta = |\frac{\epsilon^{exp} - \epsilon^{sim}}{\epsilon^{exp}}| \cdot 100\%$, with ϵ equal to the standard deviation, auto-correlation length or cross-correlation length. An overview of the statistics of the combined data set and the individual specimens are given in table 5, while these for the individual 1-D random fields are presented in table 6. The latter table also shows the experimental information regarding the individual tow standard deviation

and correlation information since this is not yet described.

Table 5: Standard deviation and correlation lengths for the combined data set and average values for the individual specimens.

	σ^{comb}	$<\sigma^{spec}>$	ξ_A^{comb}	$<\xi_A^{spec}>$	ξ_C^{comb}	$<\xi_C^{spec}>$
Warp tows [mm]	0.106	0.103	115.81	114.00	4.54	4.42
Δ_{warp} [-]	0.09%	3.48%	0.80%	0.78%	1.03%	1.72%
Weft tows [mm]	0.613	0.570	52.95	52.76	13.10	13.05
Δ_{weft} [-]	0.28%	7.38%	0.12%	0.25%	0.45%	0.87%

The standard deviation σ and correlation lengths ξ_{auto}, ξ_{cross} of the combined data set indicate that the series expansion method reproduces the experimental data within Δ=1% difference of the experimental data. The input and simulated correlation structures perfectly overlap, even for pairs of points with the largest spacing as shown in figure 10 for the warp auto- and cross-correlation structure. When fewer simulations are performed small deflections for the largest lags are present. The applied truncation given in table 4 does thus not prevent to obtain a good similarity with the target statistics.

The statistical information corresponding to the individual specimens also shows good resemblance with the target statistics. In figure 11, the histogram is shown of

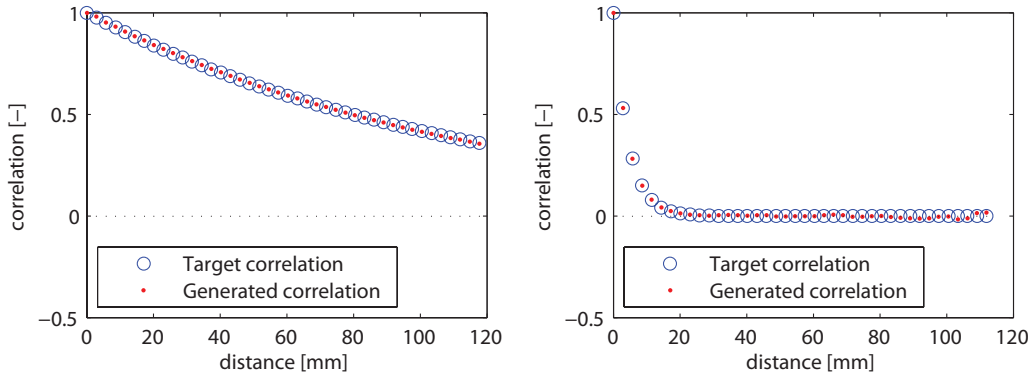

Figure 10: Comparison of the warp input and simulated auto-correlation (left) and cross-correlation (right) structure.

all simulated auto- and cross-correlation lengths for the warp tows. Similar results are obtained for the weft tows. The mean of the statistical information of all specimens has a normalised error Δ which is less than 7.4% for the standard deviation and maximum 1.72% for the correlation lengths. Although the weft deviations are only approximated by a normal distribution, the error in standard deviation is still acceptable. The large variation observed in the histograms demonstrates the large uncertainty when deriving the correlation correlation lengths.

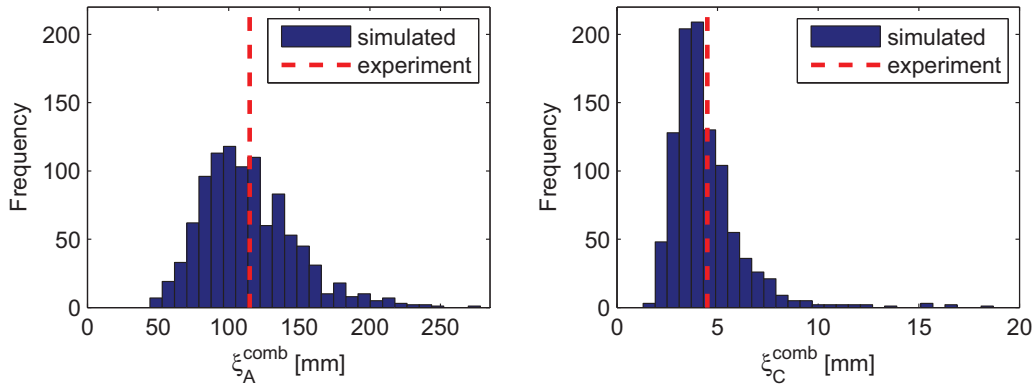

Figure 11: Simulated auto- (left) and cross-correlation (right) lengths of warp in-plane centroids.

As third comparison, the individual tows are characterised in terms of standard deviation and auto-correlation. Table 6 shows the results derived from the experimental data with mean values and coefficient of variations *cv* for the simulations. The experimental information of single tows, derived in the same manner as described in section 2, considerably deviates from the specimen statistics in table 2. The high auto-correlation in combination with a significant cross-correlation, leads to individual tow information that can significantly differ from one to another. This uncertainty is reflected in the high coefficient of variation. Especially for the correlation length, data collected from only two one-ply samples is insufficient to obtain an accurate description. The simulated standard deviations for single tows correspond very well with the experimental

information as indicated by the normalised difference Δ. The LHS sampling technique ensures that even at this level the target mean and standard deviation are achieved. In contrast to these observations, simulated correlation lengths of the 1-D random fields are only fairly reached with similar order of magnitudes. The auto-correlation length of the warp tows is overestimated, while the weft auto-correlation length is underestimated. Besides this discrepancy, the coefficient of variation *cv* is much larger than for the experiments. Various reasons, besides the limited data set size, can be raised: (i) the normality assumption of the distribution alters the single tow correlation information and (ii) the input correlation functions do not accurately represent the correlation at tow level. No effect of the fitting operation is expected since similar least-square fitting errors are obtained for fitted functions to the experimental and simulated data.

Table 6: Standard deviation and correlation lengths for individual one-dimensional random fields.

	σ^{target}	σ^{1D}	ξ_A^{target}	ξ_A^{1D}
Warp tows - *mean* [mm]	0.051	0.053	20.69	32.06
Warp tows - *cv* [-]	35.16%	36.62%	108.04%	132.00%
$\Delta_{warp,mean}$ [-]	-	2.93%	-	54.93%
Weft tows - *mean* [mm]	0.363	0.353	116.04	63.89
Weft tows - *cv* [-]	62.79%	51.36%	86.77%	154.82%
$\Delta_{weft,mean}$ [-]	-	2.67%	-	44.94%

The similarities between experiments and simulations of the in-plane centroid demonstrate that the methodology based on the Karhunen-Loève series expansion method is able to correctly reproduce the statistical information on average.

4. Discussion

Simulation results are in accordance to the statistical information of the experimental samples. The modelling procedure reproduces the input standard deviation and correlation information. A thorough characterisation of the tow path of experimental

samples is thus mandatory to achieve virtual specimens that are replicas of the physical samples. Therefore, it is important to assess the errors that are introduced when quantifying the in-plane centroid variations from the one-ply samples in [7]. The strongest assumptions are the approximated normal distribution for the in-plane deviations and the estimation of the correlation length from fitted correlation functions. In addition, uncertainty is also introduced during processing of the digital image with a resolution of 1200 DPI. The manual error in the determination of the tow boundaries is assumed to be ± 2 pixels, which corresponds to 0.042 mm. This is of similar magnitude of the standard deviation of individual warp tows and is thus not negligible. It is important to minimise these errors to have an as accurate as possible statistical description of the material.

In a next step, virtual specimens are created by a stochastic multi-scale modelling approach. The short- and long-range geometrical variability are simulated for the in-plane centroid, out-of-plane centroid, aspect ratio and area of each cross-section. Except for the in-plane deviations, all tow path parameters vary within the unit cell dimensions and are not cross-correlated with neighbouring tows. Each random reinforcement parameter is built by combination of an average trend with zero-mean deviations, using the statistical information collected in [5] and [7]. Average trends are determined from the experimental data and are the same for all realisations. Deviations are simulated using the Monte Carlo Markov Chain algorithm for textile structures [6, 20] when not cross-correlated, while the cross-correlated in-plane centroid fluctuations are produced as Gaussian random fields by applying the methodology described in section 3. A virtual model of the textile composite is obtained in the WiseTex format [21] by overwriting the original tow path information of a nominal WiseTex representation. These realistic textile models can be subsequently used for evaluating the mechanical performance, damage modelling or impregnation analysis. The general procedure of this modelling approach is addressed in a future publication.

5. Conclusions

A framework based on the Karhunen-Loève series expansion is adopted to simulate the in-plane tow path variability of textile composites. The experimental auto- and cross-correlation matrices are represented in terms of its eigenvalues- and vectors to introduce the spatial correlation information in each of the produced random series. Within a specimen, all tow centroids of equal genus are expanded using the same spectrum of eigenvectors that represent the auto-correlation structure. The sets of random variables, used for the expansion of each field, are cross-correlated with neighbouring fields to describe the positional dependency between tows. Any realisation of the in-plane path position describes the long-range geometrical variability within the textile composite. In combination with the tow path parameters varying on the short-range, realistic virtual specimens can be generated that span multiple unit cells.

The methodology is validated by simulating thousand specimens of a carbon-epoxy 2/2 twill woven composite consisting of forty warp and weft tows. In-plane deviations possess similar wavelengths as the experimental fluctuations quantified in prior work. The experimental statistical information of single specimens is reproduced with a maximum normalised error of 7.4% for the standard deviation and 1.72% for the correlation lengths, while the auto-correlation length of the individual tows are only approximated by the same order of magnitude.

Acknowledgements

This study is supported by the Flemish Government through the Agency for Innovation by Science and Technology in Flanders (IWT) and FWO-Vlaanderen.

References

[1] Mehrez, L., Doostan, A., Moens, D., Vandepitte, D.. Stochastic identification of composite material properties from limited experimental databases, part 1:

Experimental database construction. Mechanical Systems and Signal Processing 2012;27:471–483.

[2] Cox, B., Yang, Q.. In quest of virtual tests for structural composites. Science 2006;314(5802):1102–1107.

[3] Stig, F., Hallström, S.. Spatial modelling of 3D-woven textiles. Composite Structures 2012;94(5):1495–1502.

[4] Charmpis, D.C., Schuëller, G.I., Pellisetti, M.F.. The need for linking micromechanics of materials with stochastic finite elements: A challenge for materials science. Computational Materials Science 2007;41(1):27–37.

[5] Vanaerschot, A., Cox, B., Lomov, S., Vandepitte, D.. Stochastic framework for quantifying the geometrical variability of laminated textile composites using micro-computed tomography. Composites Part A 2013;44:122–131.

[6] Vanaerschot, A., Cox, B., Lomov, S., Vandepitte, D.. Stochastic multi-scale modelling of textile composites based on internal geometry variability. Computers & Structures 2013;122:55–64.

[7] Vanaerschot, A., Cox, B., Lomov, S., Vandepitte, D.. Stochastic characterisation of the in-plane tow centroid in textile composites to quantify the multi-scale variation in geometry. In: Proceedings of the IUTAM Symposium on Multiscale Modeling and Uncertainty Quantification of Materials and Structures. Santorini, Greece: Springer; 2014,.

[8] Skordos, A.A., Sutcliffe, M.P.F.. Stochastic simulation of woven composites forming. Composites Science and Technology 2008;68(1):283–296.

[9] Endruweit, A., Long, A.C.. Influence of stochastic variations in fibre spacing on the permeability of bi-directional textile fabrics. Composites Part A 2006;37(5):679–694.

[10] Abdiwi, F., Harrison, P., Koyama, I., Yu, W., Long, A., Corriea, N., et al. Characterising and modelling variability of tow orientation in engineering fabrics and textile composites. Composites Sciences and Technology 2012;72(9):1034–1041.

[11] Yushanov, S., Bogdanovich, A.. Fiber waviness in textile composites and its stochastic modeling. Mechanics of Composite materials 2000;36(4):297–318.

[12] Vořechovský, M.. Simulation of simply cross correlated random fields by series expansion methods. Structural Safety 2008;30(4):337–363.

[13] Hexcel, . HexForce G0986 SB 1200. 2012.

[14] Vanmarcke, E.. Random Fields: Analysis and Synthesis. MIT press, Cambridge; 1993.

[15] Ghanem, R., Spanos, P.. Stochastic Finite Elements: a Spectral Approach. New York: Springer-Verlag; 2000.

[16] Sudret, B., Kiureghian, A.D.. Stochastic finite element methods and reliability: a state-of-the-art report. Department of civil & environmental engineering, University of California Berkeley; 2000.

[17] Guilleminot, J., Soize, C., Kondo, D., Binetruy, C.. Theoretical framework and experimental procedure for modelling mesoscopic volume fraction stochastic fluctuations in fiber reinforced composites. International Journal of Solids and Structures 2008;45(21):5567–5583.

[18] Chen, N., Soares, C.G.. Spectral stochastic finite element analysis for laminated composite plates. Computer Methods in Applied Mechanics and Engineering 2008;197(51).

[19] Vořechovský, M., Novák, D.. Correlation control in small-sample monte carlo type simulations 1: A simulated annealing approach. Probabilistic Engineering Mechanics 2009;24(3):452–462.

[20] Blacklock, M., Bale, H., Begley, M., Cox, B.. Generating virtual textile composite specimens using statistical data from micro-computed tomography: 1D tow representations for the Binary Model. Journal of the Mechanics and Physics of Solids 2012;60(3):451–470.

[21] Verpoest, I., Lomov, S.V.. Virtual textile composites software wisetex: Integration with micro-mechanical, permeability and structural analysis. Composites Science and Technology 2005;65(15-16):2563–2574.